Wide-Range Autonomous Ingress Tactical Hunter (WRAITH) Aerodynamic Redesign

Tri Phan[1], Nathaniel Hollman[2], Tiger Sievers[3] and Mohamed Almazrouei[4],
University of Kansas, Lawrence, Kansas, 66045, United States

I. Executive Summary

This report discusses the aerodynamics of the WRAITH missile, an updated version of the JASSM developed by Lockheed Martin. First, an operational range of speeds and altitudes were researched and postulated to develop the range of conditions the missile will experience. The missile was found to cruise at an altitude of 2,000-30,000 ft at Mach 0.71. The mission the WRAITH will fly is being launched at high altitude and high speed and lowering its altitude to a low cruising altitude to avoid radar before hitting the target. A model of the atmosphere was developed, and the dynamic pressure ranges that the WRAITH will experience were calculated. The body aerodynamic center of the missile then calculated and considered at different angle of attack, which is determined to be close to the nose in cruise flight and moving towards aft as angle of attack increases. The aerodynamics of the missile drag produced by the body are then calculated, with the major contributions being from friction drag, due to the missile being subsonic. The normal forces from angle of attack were then calculated for the missile, and the maximum lift to drag ratios were found. Because of the high aspect ratio of the wing and the subsonic cruising conditions, lifting surface theory was chosen to analyze the planar surfaces. Since the missile only experienced subsonic flight, drag due to friction was the only one analyzed. The tail size was determined to be zero, making the missile have a flying wing design. With that, the C.G. location could be determined to result in a tailless design.

[1] Responsible for Lift over Drag and Cruise Conditions.
[2] Responsible for Body Forces and MAC.
[3] Responsible for Tail Forces and MAC.
[4] Responsible for Wing Forces and MAC.

II. Background

The Wide-Range Autonomous Ingress Tactical Hunter (WRAITH) is a stealthy, precision-guided cruise weapon designed to be launched from stand-off ranges, fly at low observable altitude, with terrain following profile to penetrate enemy air defenses, and deliver a high-explosive warhead onto a fixed target with guided terminal homing. In this design, we retain the Lockheed Martin JASSM's baseline mission and guidance suite but replace the conventional horizontal tail surfaces with a streamlined boattail rear fuselage and optimized aft control fins if needed. The boattail reduces radar and aerodynamic drag while shifting stability and trim requirements rearward. This configuration aims to preserve low observable characteristics and range while trading some longitudinal stability for improved cruise efficiency and simpler external signatures.

Table 1 The WRAITH Specifications

Baseline Design	Old Dimension	New Dimension
Body Diameter	21.61 in	21.61 in
Reference Area	369.25 in^2	369.25 in^2
Nose Length	40.68 in	40.68 in
Total Body Length	161.95 in	161.95 in
Elliptical Height	10.00 in	10.00 in
Elliptical Width	11.67 in	11.67 in
Roll Angles	0 deg	0 deg
Nose-tip Diameter	0 in	0 in
Center of Gravity Assumption	0.5 total length	0.5 total length
Effective Exhaust Area	23.76 in^2	23.76 in^2
Leading Edge Section Angles	0 deg	0 deg
Number of Surfaces	3	3
Sweep Angles	45 deg	45 deg
Wingspan	7.87 ft	9 ft
Root Chord Length	1.00 ft	1.00 ft
Nose Tip to Root Chord Leading Edge of Wing	60.6 in	60.6 in
Tail Area	0 ft^2	3.36 ft^2

Much of this geometry was found using a three-view of the JASSM rocket and using the total length as a base dimension [1]. The missile body was modeled in NX to measure the other derived geometry [2]. The main thing that was changed from the JASSM to the WRAITH was that the wingspan increased, which increases the lift to drag due to less drag from higher span, and less lift coefficient is required at cruise. The other major change was from a conventional tail to a V-tail which was made to increase yaw and pitch controllability as the missile needs to react faster due to proximity to terrain.

A. Mission Description

This report will observe these initial conditions and flight regime, specifically when discussing the dynamic pressure and Mach plots, as these conditions force the missile into vastly different circumstances. The WRAITH is launched at high altitude of 40,000 ft at Mach 0.9 from either a fighter jet or a B-1 Lancer. The theory behind this is that the aircraft is in supersonic flight and slows to Mach 0.9 to launch the WRAITH without forcing the missile into an unusual Mach range. The WRAITH then coasts down to 30,000 ft with its wings deployed to save fuel and increase range and then begins powered flight while descending to 2,000 ft. The missile will aim to cruise at 2000 ft at 0.71 Mach to avoid radar detection to remain stealthy. When near the target, the WRAITH will decelerate a little to 0.6 Mach and will climb to 3,000 ft and will finally accelerate when descending to hit its target, reaching a speed of around Mach 0.9.

Operational Cruise Mach number: 0.71
Maximum Mach number: 0.9
Cruise altitude: 2000 ft – 30,000ft [3] and [4]
Operational AoA: less than 10 deg
Stall Effective AoA: 30 deg

III. Standard Atmosphere

The standard atmosphere was found using an online resource which provided the ratios of temperature, pressure, and density for increasing altitudes in kilometers [5]. A function was then created to interpolate this data, which was previously extracted to a .mat file for code efficiency. Atmospheric data was found for up to 80,000 feet in altitude, and the ratios of pressure, temperature, density, and the speed of sound are shown in Figure 1. Note that this data is the temperature states static values, or the stream values if observed at zero velocity.

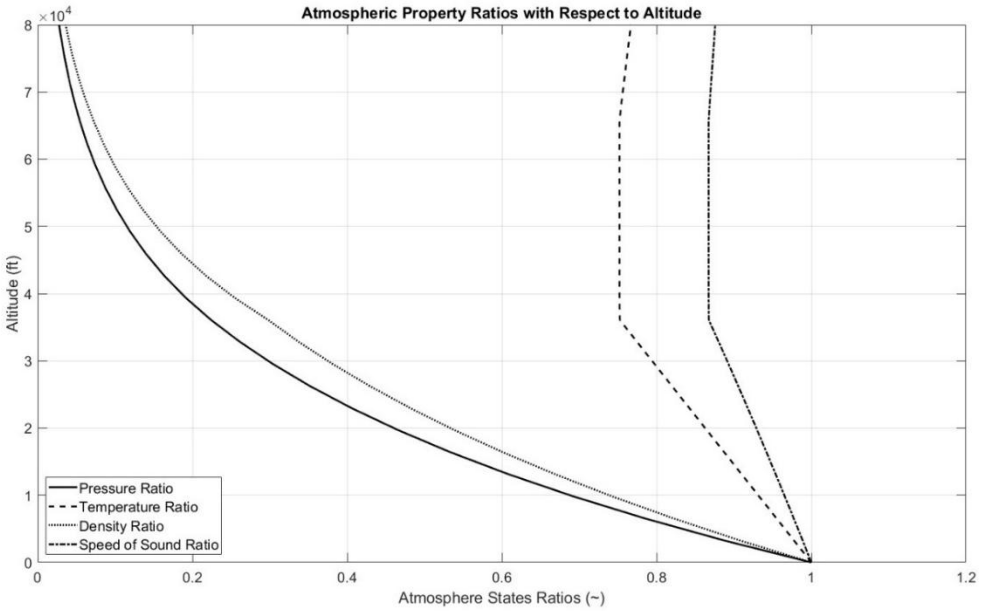

Figure 1 Standard Atmospheric State Ratios for 80,000 ft

These ratios are a multiplier of the local sea level absolute states. The standard sea level states were researched and found to be pressure = 14.7 psi, temperature = 518.7˚R, density = 0.002377 lb/ft^3, and the speed of sound = 1,117 ft/s. In general, pressure and density decrease with altitude and approach zero as they reach the boundary of space. Temperature decreases until around 40,000 ft, where it stays constant until around 65,000 ft where it starts increasing due to less protection from the sun. It was assumed for this that the gas constants did not change with altitude, so the speed of sound ratio varied to the square root of the temperature. While this is an inaccurate assumption, for our true operational altitude, these values will minimally change, meaning that the assumption is not inaccurate for our operational ranges. With a defined ceiling of 40,000 ft, the plot of the states can be narrowed to the operational range in Figure 2.

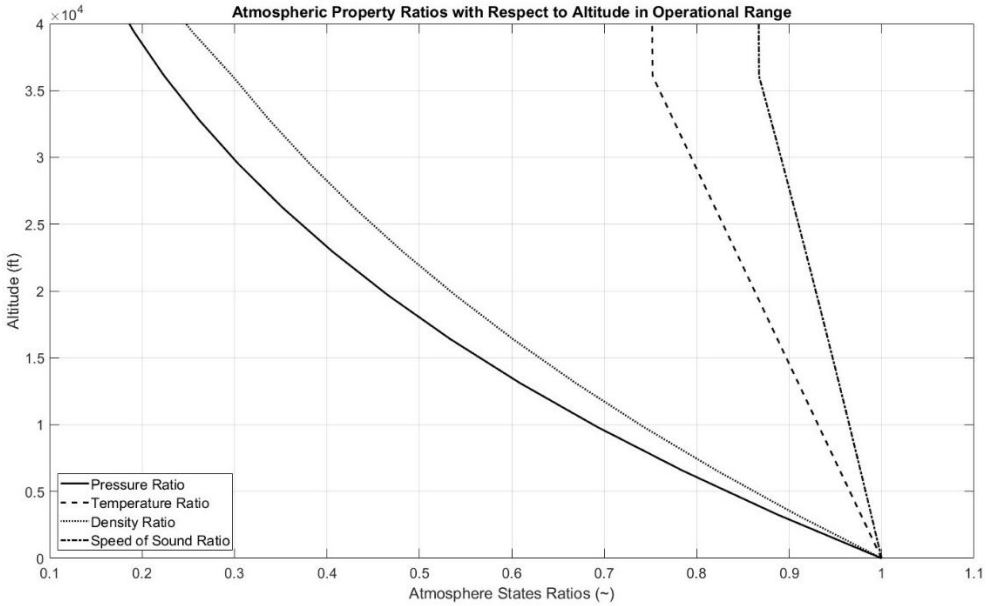

Figure 2 Standard Atmospheric State Ratios for Operational Range

The speed of sound ratio was then used to find the average Mach value for the operational range, which was found by averaging the ratio of the speed of sound and multiplying it by the ground speed of sound velocity. This yielded an average speed of sound of 1037 ft/s. The dynamic pressure can then be calculated for the operational range of Mach numbers using this average speed of sound and the change in density through altitude. The contours for these are shown for a range of Mach numbers in Figure 3.

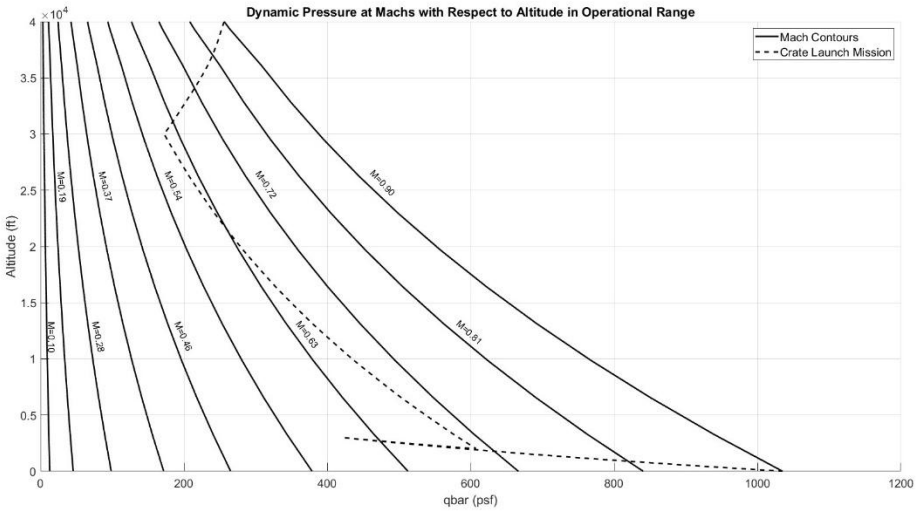

Figure 3 Dynamic Pressures at Various Mach Numbers and Altitudes

This plot also shows the two previously described missions flown in terms of altitude and dynamic pressure. Note that for different missions, the WRAITH must be within a dramatically different range of dynamic pressures as its altitude and Mach speed vary significantly. This shows how the controller for the WRAITH must consistently adapt to its current conditions, and the aircraft itself

must be robust enough to fly at these varieties of conditions. As previously mentioned, in mission 1 the WRAITH is launched at slow speed at low altitude from a parachute-suspended crate and descends to the cruise altitude of 2,000 ft at Mach 0.71. Mission 2 is when the WRAITH is launched from a high altitude at a fast speed, such as from an F-22 at 40,000 ft, where it coasts to a lower speed, and then cruises to its point of Mach 7.1 at 2,000 ft. After this, it is estimated that on its descent to its target, it could reach a speed of Mach 0.9, so this is done to demonstrate the farthest extent of the dynamic pressure that the WRAITH could experience. This entire range describes how the WRAITH must be able to have a powerful enough control surface to maneuver at low dynamic pressures, while having an accurate enough surface to make minute adjustments at high dynamic pressures. Figure 4 combines the pressure and temperature ratios for the operational atmosphere, as well as the dynamic pressure normalized to the maximum dynamic pressure of 1034.9 psf.

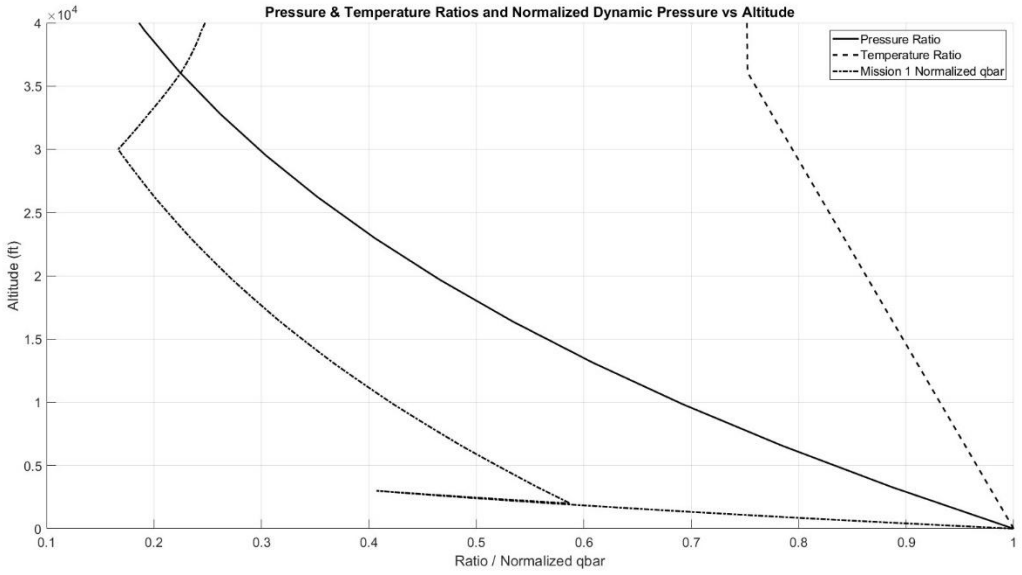

Figure 4 Combined Atmosphere and Normalized Dynamic Pressure Plot

It is seen that the minimum dynamic pressure is at when the aircraft stops coasting to a lower altitude and begins the burn to its cruising altitude.

V. Mean Aerodynamic Center

B. Body Mean Aerodynamic Center

The mean aerodynamic center for the fuselage of a missile is usually around the length of the nose but varies due to changing angle of attack. This behavior is defined using the following formula.

$$X_{AC_{body}} = l_{nose}\left(0.63(1-\sin^2(\alpha)) + 0.5\left(\frac{l}{l_{nose}}\right)\sin^2(\alpha)\right)$$

The aerodynamic center of the body is then found for all the angles of attack in the range from 0 to 30 degrees, and this is shown in Figure 5.

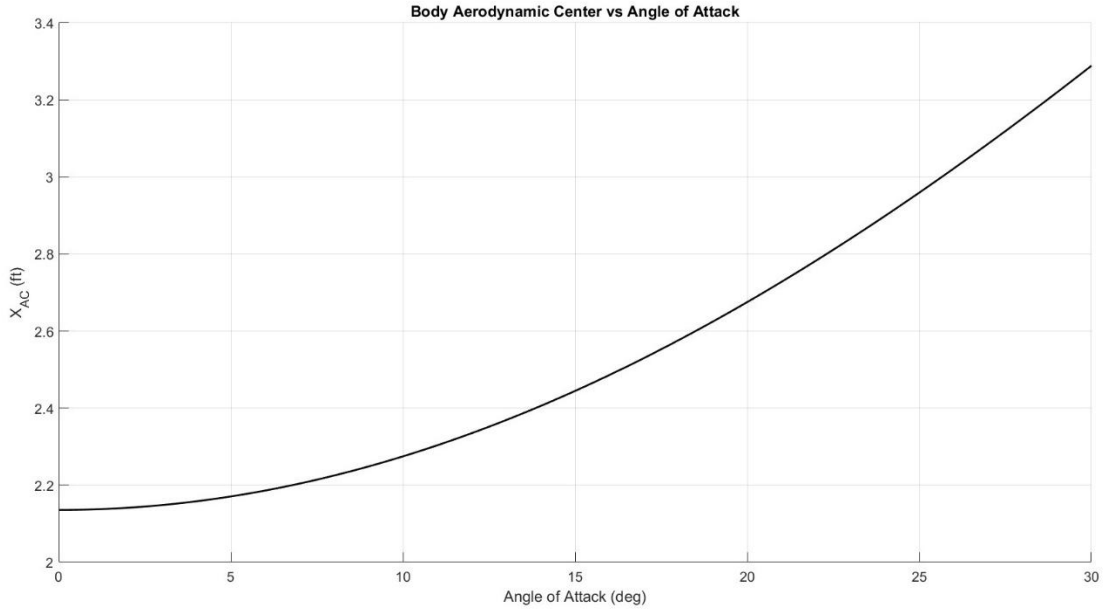

Figure 5 Body Aerodynamic Center per AoA

It is seen that as the angle of attack increases, the mean aerodynamic center of the body moves from 2.2 feet from the nose tip to around 3.3 feet from the nose tip. Note that this is proportional to the magnitude of the angle of attack, so if the WRAITH experiences a negative angle of attack of 30 degrees, the MAC will be at 3.3 feet from the nose tip.

C. Total Mean Aerodynamic Center

The mean aerodynamic center for the WRAITH was determined using the following equation,

$$x_{ac,total} = \frac{C_{N_\alpha,b}\, x_{ac,b} + C_{N_\alpha,w,eff} x_{ac,w} + C_{N_\alpha,t,eff} x_{ac,t}}{C_{N_\alpha,total}}$$

Which sums up the contributions to lift from each of the lifting components and the individual aerodynamic center to find the total aerodynamic center. The resulting aerodynamic center for the missile at cruise is shown in Figure 6.

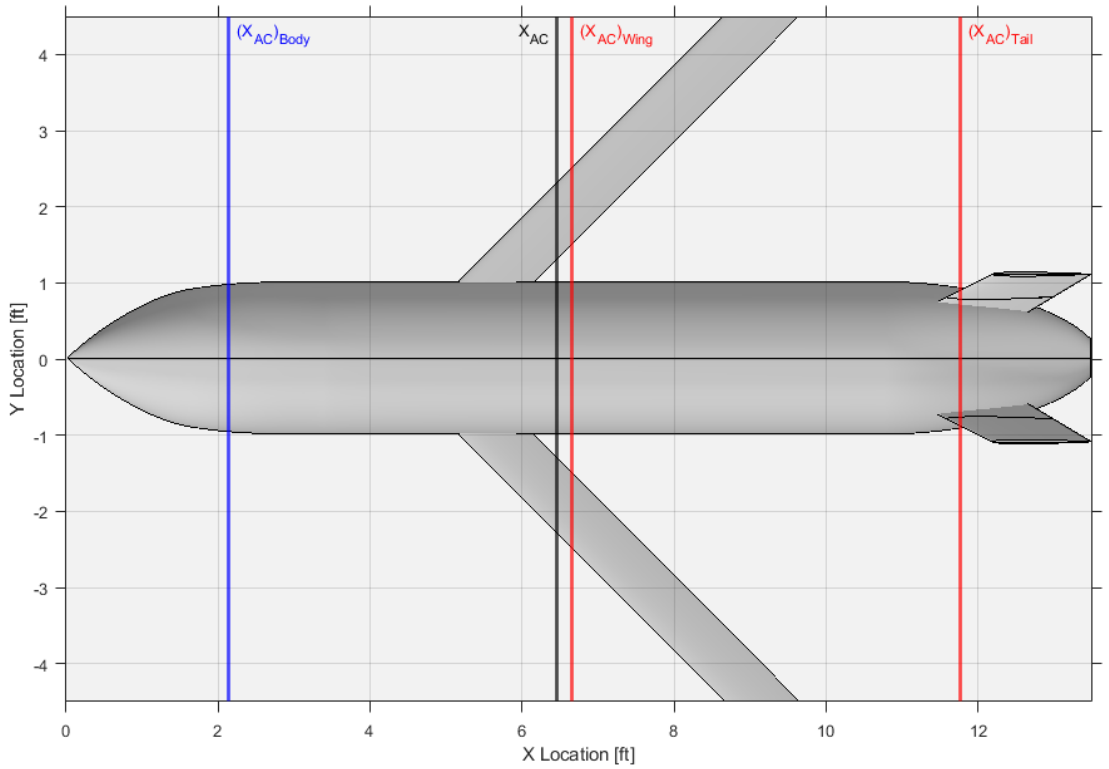

Figure 6 Mean Aerodynamic Center at Cruise Conditions

Increasing the angle of attack results in a rearward shift of the aerodynamic center. This is impacted largely by the shift in the body aerodynamic center, characterized by the body aerodynamic center equation. The aerodynamic center of the body is highly dependent on the angle of attack. This is clearly shown in Figure 5, with the body aerodynamic center showing a noticeable shift from 1 to 30 degrees. Planar surfaces show minimal shift in the aerodynamic center. Below Mach 0.7, the aerodynamic center is assumed to be $0.25\bar{c}$. This is illustrated in Figure 7, with the wing and tail showing no shift due to angle of attack.

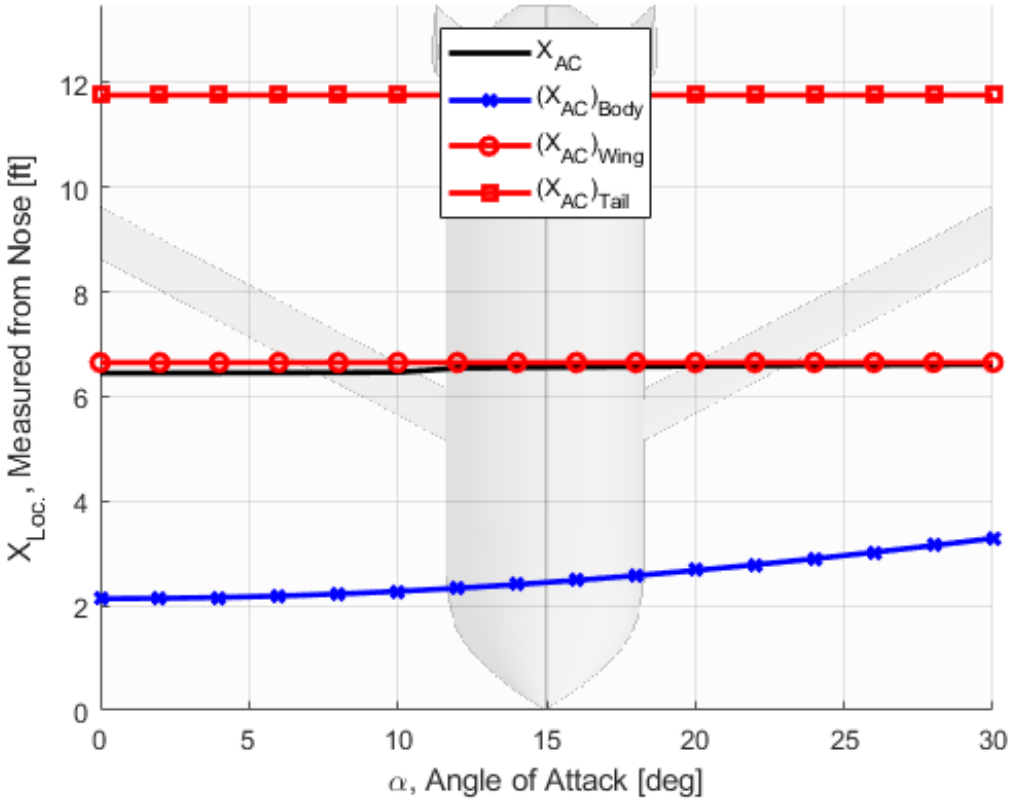

Figure 7 Aerodynamic Center Shift due to Angle of Attack

Overall, the aerodynamic center of the missile is dominated by the large wing, with the body and tail having minor contributions overall. The jump in aerodynamic center at 10 degrees is due to the discontinuity in the equations used for planar normal forces at high and low angles of attack. This increases the contribution of the wing and tail, in turn causing the increase in the aerodynamic shift. The equations describing this behavior are shown below.

Wing

$$C_{N_\alpha} = \frac{2\pi\,\mathrm{AR}}{2 + \sqrt{\mathrm{AR}^2(1 + \tan^2\Lambda_{\mathrm{LE}}) - M^2 + 4}} \qquad \text{for } \alpha' < 10^\circ$$

$$C_N = \left[\frac{2\pi\,\mathrm{AR}}{2 + \sqrt{\mathrm{AR}^2(1 + \tan^2\Lambda_{\mathrm{LE}}) - M^2 + 4}}\,|\sin\alpha'\cos\alpha'| + 2\sin^2\alpha'\right]\left(\frac{S_{\mathrm{surf}}}{S_{\mathrm{ref}}}\right) \qquad \text{for } \alpha' > 10^\circ$$

Tail

$$C_{N_\alpha} = \frac{\pi A_T}{2} \qquad \text{for } \alpha' < 10^\circ$$

$$C_N = \left[\left(\frac{\pi\,\mathrm{AR}}{2}\right)|\sin\alpha'\cos\alpha'| + 2\sin^2\alpha'\right]\left(\frac{S_{\mathrm{surf}}}{S_{\mathrm{ref}}}\right) \qquad \text{for } \alpha' > 10^\circ$$

VI.Drag

D. Body Drag

Recalculating the body drag from the baseline includes the incorporation of the boattail as a drag reduction method. By tapering the end of the missile, the base area of the tail is reduced from the reference area. To update the equation according to the boattail, a new base drag fraction must be created. The theory behind the equation is that if the actual base area made by reducing the diameter from the boattail angle is equal to the exhaust area with engine on, then there is essentially no base drag. The following equation reflects this relationship, and if the engine is turned off, the equation becomes the next equation.

$$\left(C_{D_0}\right)_{base} = \left(\frac{A_B - A_E}{S_{ref}}\right)(0.12 + 0.13 * M^2)$$

$$\left(C_{D_0}\right)_{base} = \left(\frac{A_B}{S_{ref}}\right)(0.12 + 0.13 * M^2)$$

All that is needed then is to find the area of the boattail. To do this, the boattail angle and the tail length must first be found. Using CAD, the start of the tail was found using 95% of the height of the missile, and the boattail was calculated by taking the average of the angle from the top of the start of the tail to the top of the exhaust, and the bottom of the start of the tail to the bottom of the exhaust. It was found that the boattail angle was approximately equal to 12.5 degrees, and this is shown in Figure 8. As the area decreases to the exhaust area, the effective area was set equal to the base area to find the length of the tail.

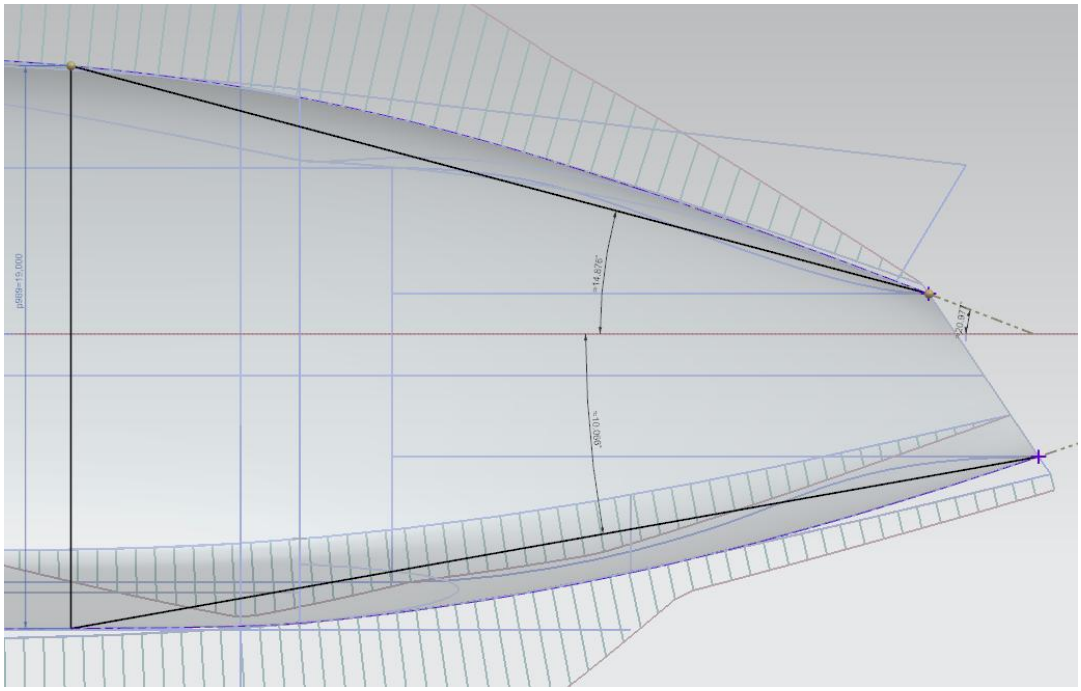

Figure 8 Boattail Geometry Calculation

Using the following equation then, the length of the tail was calculated to be 1.223 ft.

$$l_t = \frac{\left(d - \sqrt{\frac{4A_e}{\pi}}\right)}{2\tan\theta_{BT}}$$

However, since the WRAITH has a sharp edge at the exhaust of the jet, the base area will be the same as the exhaust area. The one factor that must be checked is if there is flow separation due to the angle of the boattail. The textbook says that round 10 degrees of boattail is the highest amount before flow separation occurs. However, in the figure, this only becomes a problem in transonic regions. Since the WRAITH has a maximum speed of Mach 0.9, this will not be an issue. To double check that there is no flow separation, preliminary CFD was performed to discover if flow separation occurs. It was then noted using Figure that there is no flow separation except at the exhaust due to the engine being off, and so the boattail should follow the previous equation.

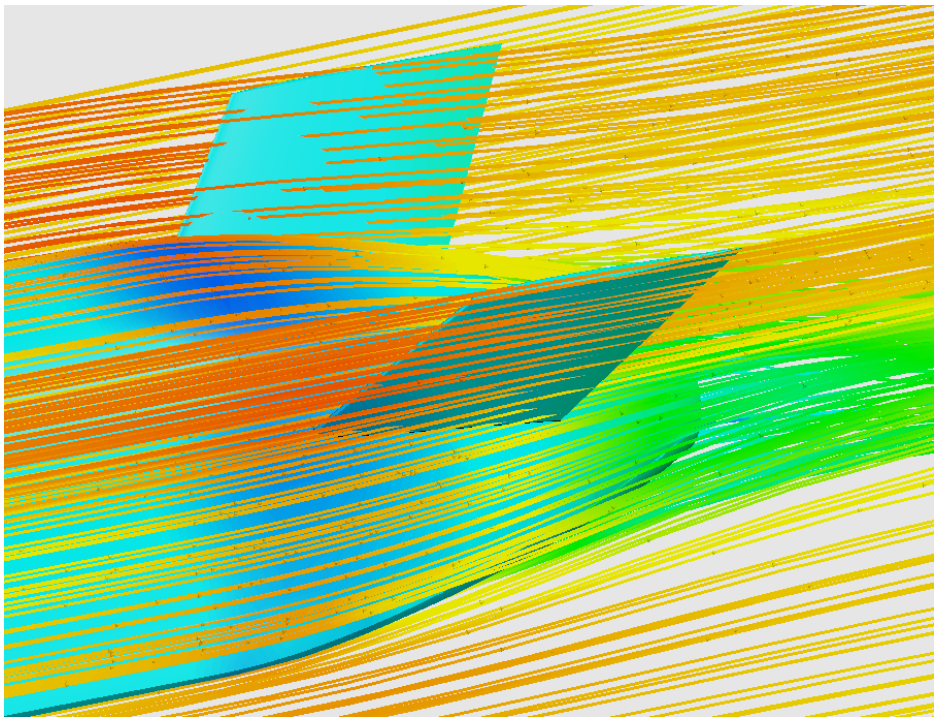

Figure 9 WRAITH Tail CFD

Using these principles, the base drag can be calculated. Since the WRAITH only flies in the subsonic range, there is no need to account for wave drag. That means the only drag left to observe is friction drag, found using the following equation.

$$\left(C_{D_0}\right)_{Body,Friction} = 0.053\left(\frac{l}{d}\right)\left(\frac{M}{ql}\right)^{0.2}$$

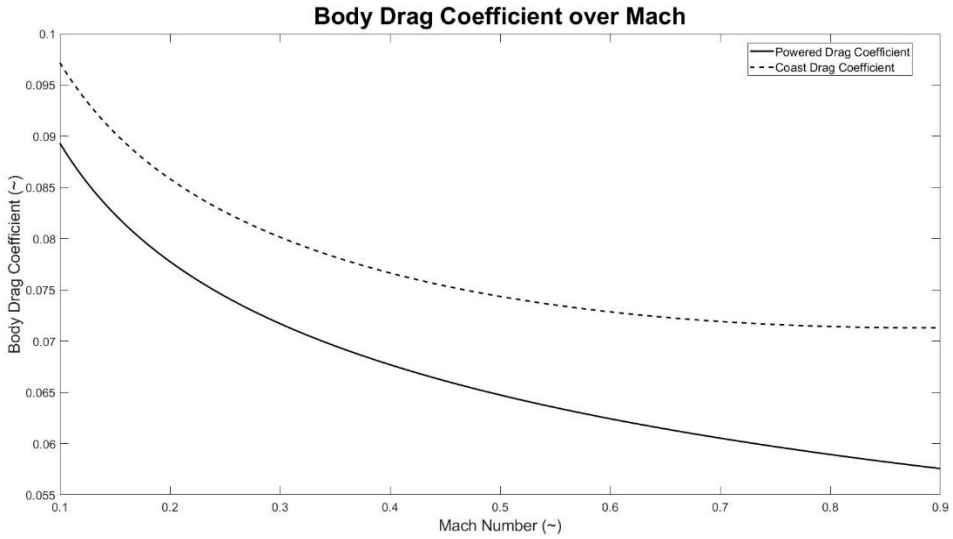

Figure 10 Body Drag per Mach Number

It is seen that the drag coefficient for powered flight is only decreasing, which makes sense as the base drag is essentially zero due to no flow separation.

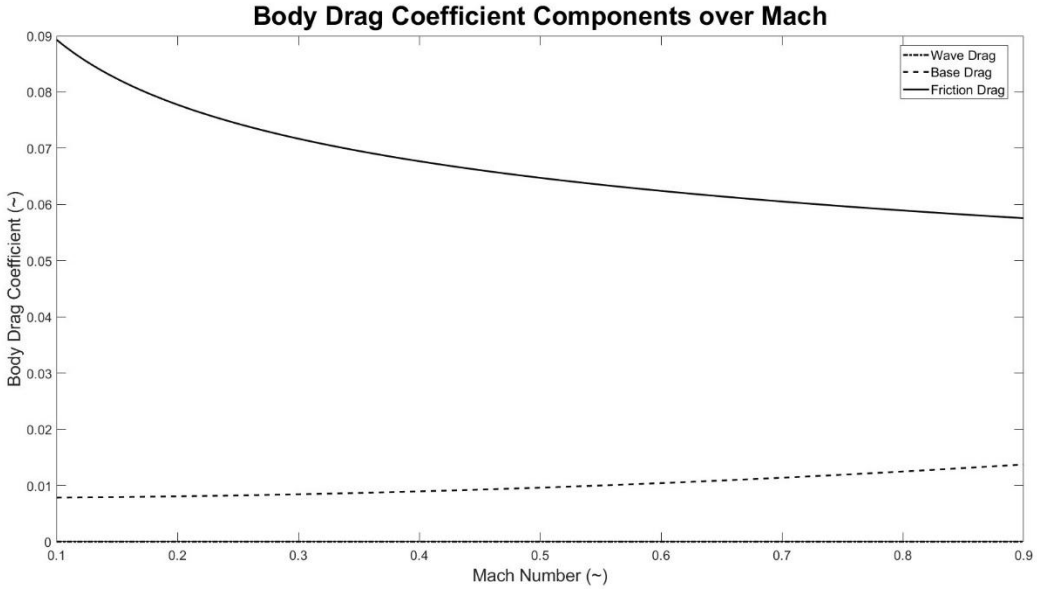

Figure 11 Coast Body Drag Components

The components for the coasting drag make sense, as the base drag area where flow separates is the size of the exhaust area, which is relatively small. This means that the base drag should be smaller than the friction drags. Note that base drag increases with speed while friction drag decreases with speed, which makes sense from according to the equations.

E. Wing Drag

For the redesigned configuration, the wingspan increased from 7.87 ft to 9 ft to extend the range of the missile. This change increased the aspect ratio of the wing, resulting in smoother airflow, reduced induced drag.

Figure 12 presents the variation of the wing's zero-lift drag coefficient C_{w0D} with Mach number. As Mach increases from 0.1 to 0.7, the friction drag decreases due to reduced skin friction effects and thinner boundary layers at higher speeds. The redesigned wing's higher aspect ratio helps minimize induced drag and contributes to a smoother aerodynamic profile. Overall, the C_{w0D} values are lower compared to the original configuration, reflecting an improvement in lift to drag ratio (L/D) and better cruise performance.

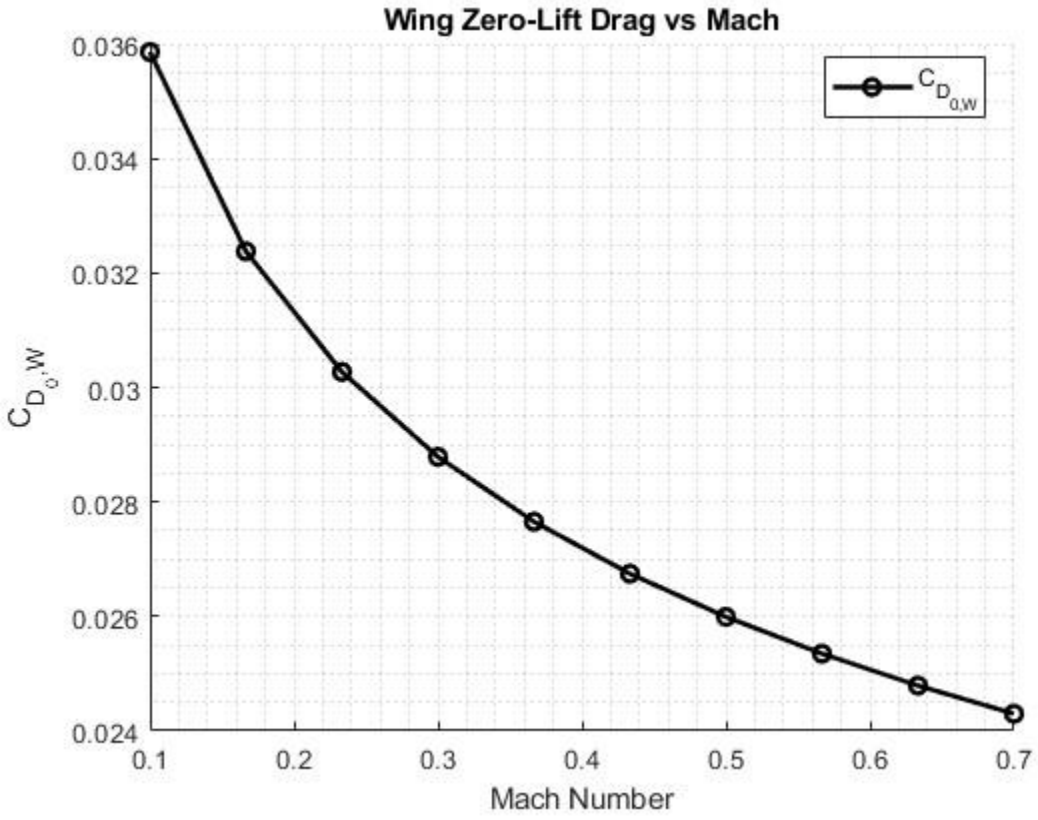

Figure 12 Wing Drag Vs. Mach

F. Tail Drag

The redesigned tail has an increased area of 3.36 ft^2, compared to the baseline 1.82 ft^2. This causes a moderate increase in drag due to friction. Using the planform friction equation described previously, Figure 13 was produced, showing the drag contribution of the tail over the flight envelope. The figure clearly shows an increase in drag, consistent with the change in planar area.

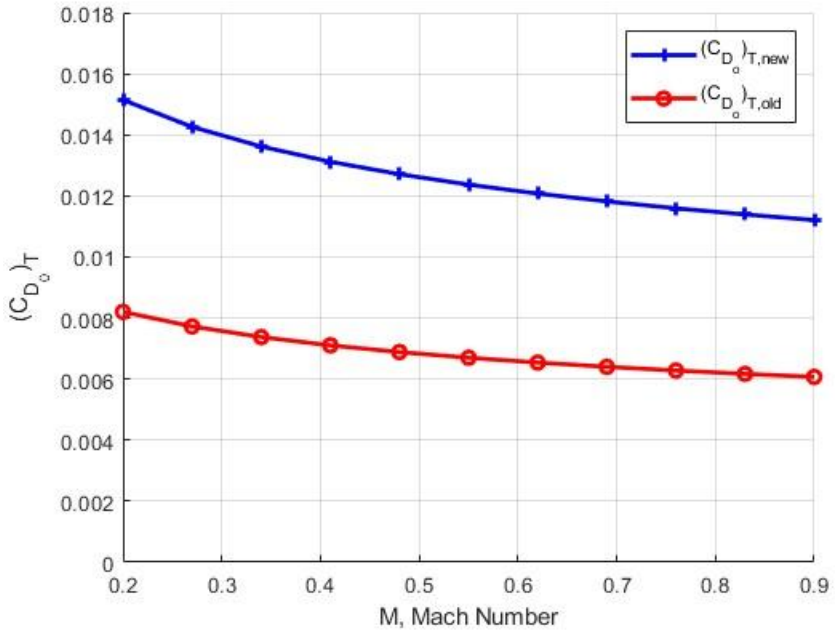

Figure 13 Tail Drag Comparison

This increase in drag is relatively small and is considered worth the cost of additional controllability.

G. Total Drag

The total drag coefficient of the WRAITH is found by summing the drag coefficients from each component. Figure 14 shows these contributions over the changing Mach number.

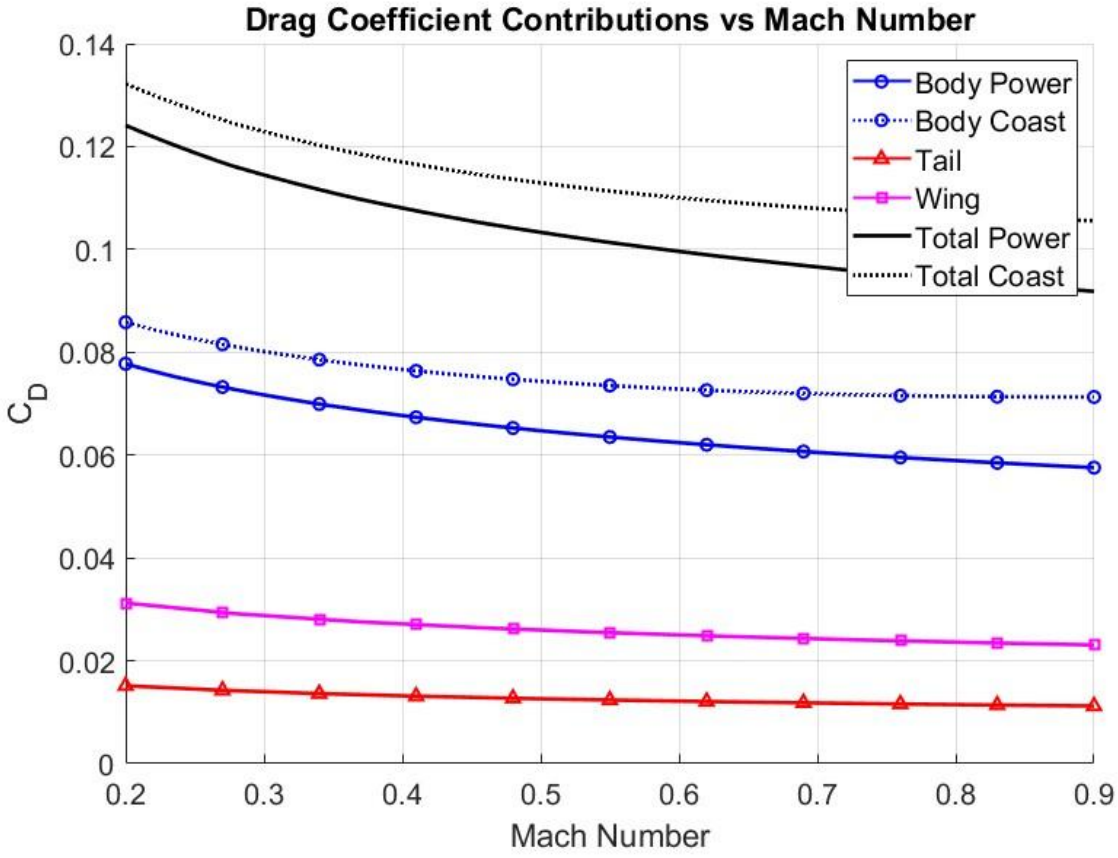

Figure 14 Drag Contributions over Mach Number

VII. Lift

H. Body Lift

The normal force produced by the body is a function of the angle of attack, roll angle, and approximated elliptical body geometry. Below is the equation for body normal force for a range of angles of attack and roll angles.

$$C_{N_{Body}} = \left(\frac{a}{b}\cos^2(\phi) + \frac{b}{a}\sin^2(\phi)\right)\left(\left|\sin(2\alpha)\cos\left(\frac{\alpha}{2}\right)\right| + 1.3\frac{l}{d}\sin^2(\alpha)\right)$$

Using this equation for the range of angles of attack and roll angles, and the plot for this is shown in Figure .

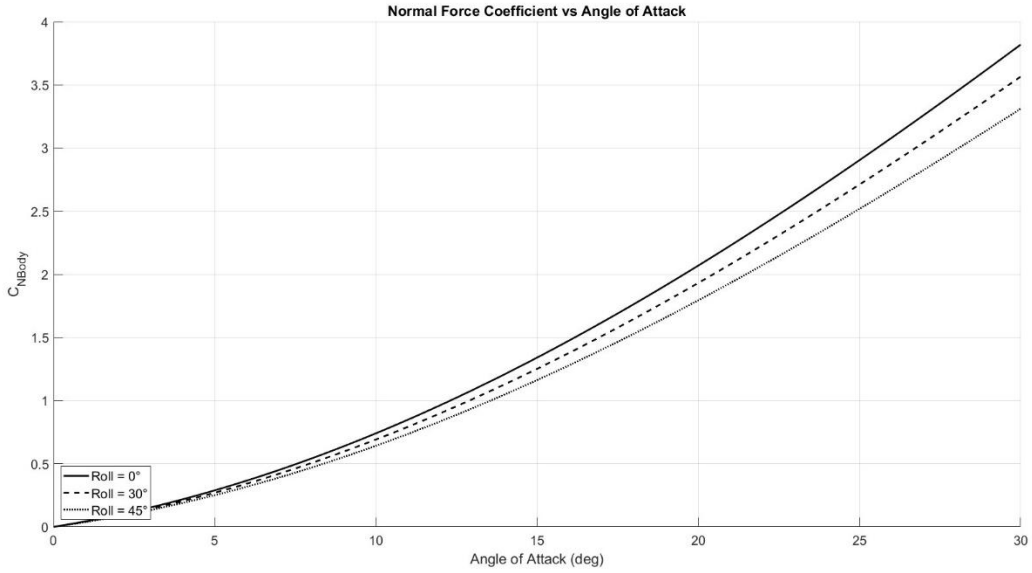

Figure 15 Body Normal Coefficient Range

It is observed that as expected, the angle of attack has a direct relationship with the normal force, and it is almost linear. Note also that since there is less cross-sectional area on the side of the missile, as it rolls it loses body lift.

I. Wing Lift

Since the WRAITH wing has a relatively large aspect ratio, it can be modeled using the linear lifting surface theory. Normal force slope $\boldsymbol{C_{N\alpha}}$ is directly related to lift curve slope $\boldsymbol{C_{L\alpha}}$. Based on that we can use small angle approximation $\boldsymbol{C_{N\alpha} \approx C_{L\alpha}}$, normal force is treated as a linear function for $\boldsymbol{\alpha < 10\, degrees}$. For the redesigned wing, the analysis was extended to α=30 degrees to study near-stall behavior. Figure 16 shows the normal force produced by the wing over different Mach numbers.

$$(C_{N_\alpha})_{\text{surface}} = \frac{dC_N}{d\alpha} \approx \frac{dC_L}{d\alpha} = \frac{2\pi A}{2 + \sqrt{A^2\left(1 + \tan^2 \Lambda_{LE}\right) - M^2 + 4}} \quad [\text{rad}^{-1}]$$

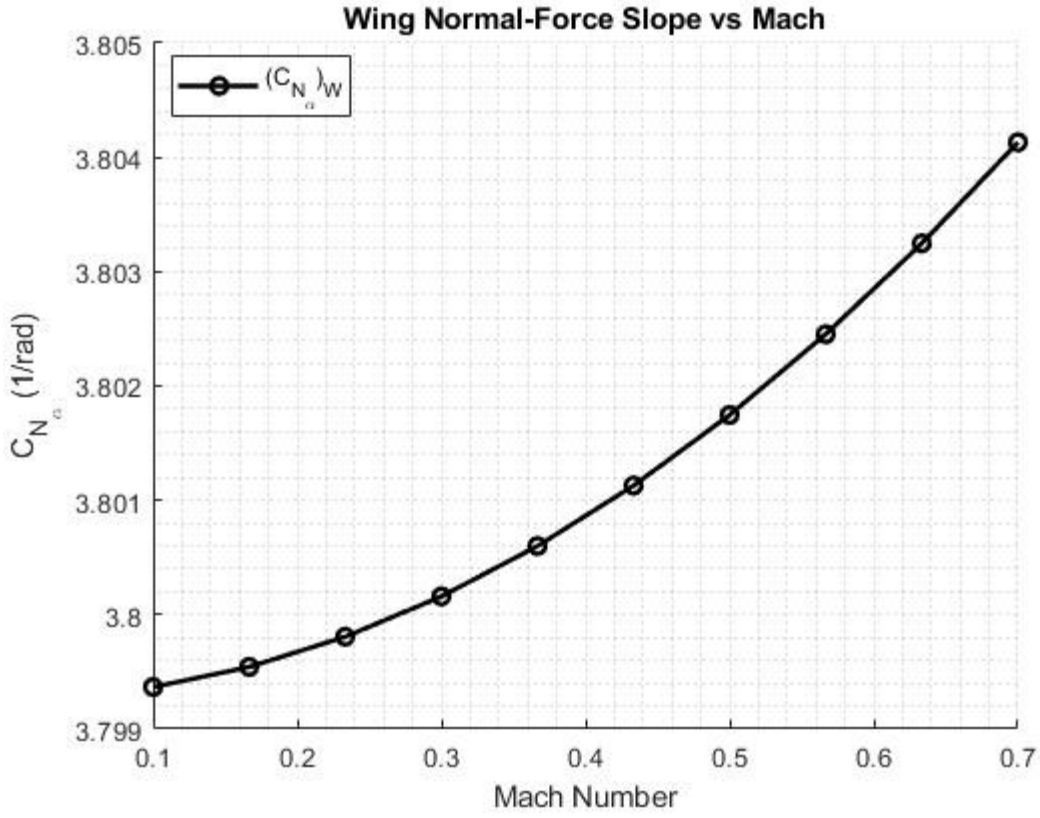

Figure 16 Normal Force Slope Vs. Mach

After determining the normal-force slope $\boldsymbol{C_{N\alpha}}$, the wing's normal-force coefficient for the redesigned configuration was modeled across both low and high angles of attack. The wingspan increased from 7.87 ft to 9 ft, so aspect ratio improved lift efficiency while maintaining low drag. To capture behavior near the stall, the analysis range for angle of attack was extended from 10° to 30°.

For small angles ($\alpha < 10$), the flow remains attached and follows the linear relation:

$$C_{N,W} = (C_{N\alpha})W\alpha$$

At higher angles ($\alpha < 10$) where partial flow separation occurs; the nonlinear effect is modeled using the following equation:

$$C_N = \left[\frac{2\pi\,\mathrm{AR}}{2 + \sqrt{\mathrm{AR}^2(1 + \tan^2\Lambda_{\mathrm{LE}}) - M^2 + 4}}\,|\sin\alpha'\cos\alpha'| + 2\sin^2\alpha'\right]\left(\frac{S_{\mathrm{surf}}}{S_{\mathrm{ref}}}\right) \quad \text{for } \alpha' > 10°$$

This equation shows the change after 10° because of the flow separation. The extended analysis provides a more accurate prediction of aerodynamic performance across the missile's subsonic flight profile. Figure 17 shows the change in normal force coefficient for different angles of attack.

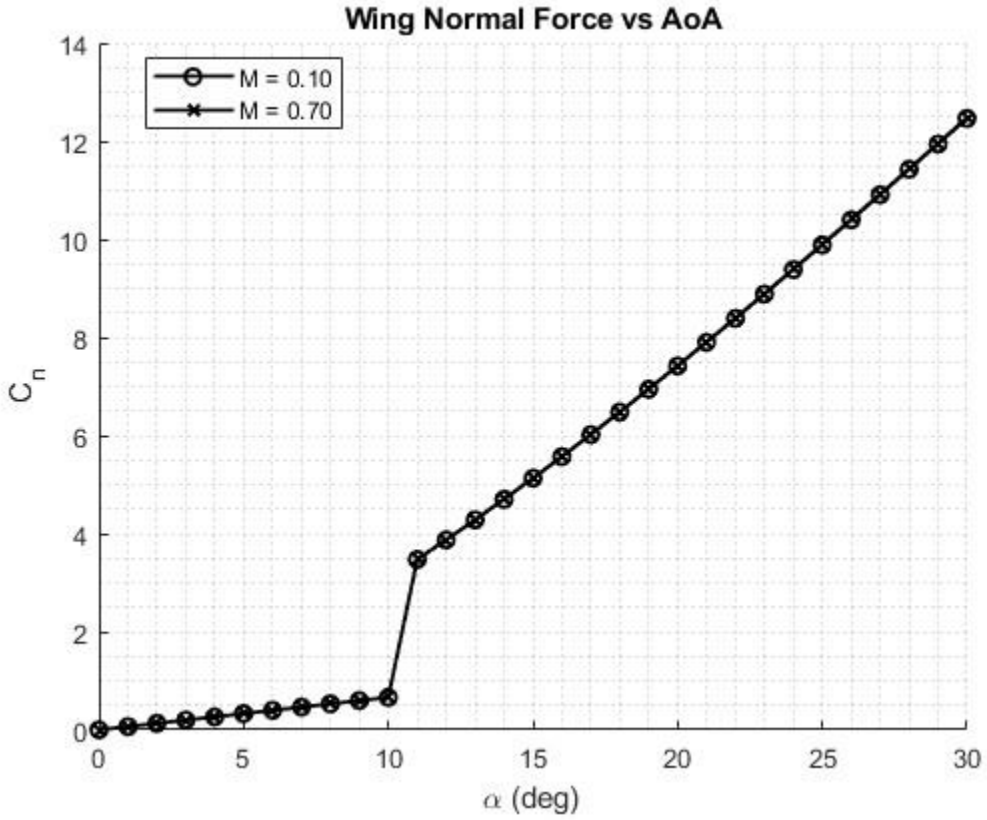

Figure 17 Wing Normal Force Vs. AOA

Figure 17 shows how the normal force coefficient for the wing varies with angle of attack up to 30°. The linear trend across Mach numbers confirms stable aerodynamic behavior within the small angle range. Increasing the wingspan from 7.87 ft to 9 ft slightly steepens the slope of C_n improving lift efficiency while maintaining low drag. The response remains linear up to about 10°, consistent with lifting surface theory, before minor nonlinear effects begin to appear at higher angles.

J. Tail Lift

The redesigned tail now produces a normal force when previously it did not, caused by the dihedral of the tail. The contributions of the vee-tail to the equivalent normal force coefficients are described below.

$$\left(C_{N_{\alpha,HT}}\right)_{eq} = \left(C_{N_\alpha}\right)_T sin^2(\phi)$$

Using the low aspect ratio equations for planar normal force, and applying the relationship above,

$\left(C_{N_{\alpha,HT}}\right)_{eq} = 1.132\ [1/rad]$.

The previous tail did not produce any normal force.

K. Total Lift

The total lift per angle of attack can then be found by adding them. The total normal force coefficients and the component contributions are shown below in Figure 18.

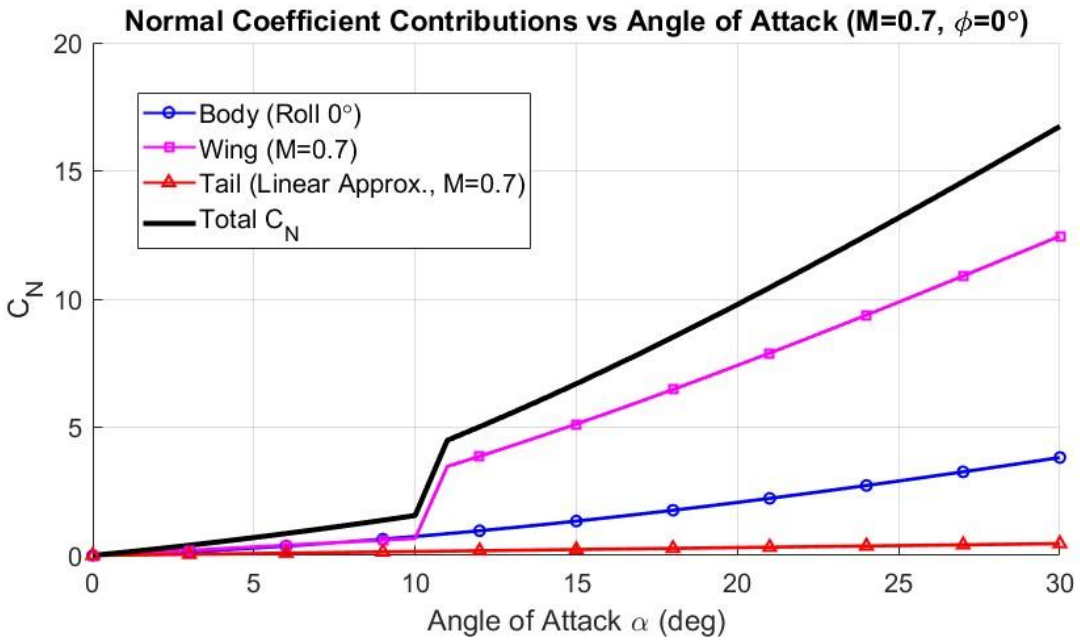

Figure 18 Total Lift per Angle of Attack

VIII. Lift-Over-Drag

In Table 2 and Figure 19, an evaluation of the body aerodynamic efficiency is conducted to the updated model. The body lift to drag ratio (L/D) is calculated as a function of angle of attack α for roll angles $\phi = 0\ deg$. Additionally, the L/D chart is generated at varying Angles of Attack up to a stall effective angle of attack of 30 deg and variety of Mach numbers based on different C_{D_0}.

Table 2 Body L/D over different Angle of Attack and Mach Number

$Mach\ numbers$	$\left(\frac{L}{D}\right)_{max}$

0.1	3.29
0.5	3.65
0.7	3.73
0.9	3.78

The cruise speed is estimated to be 0.71 and cruise body angle of attack around 8 degrees for the best lift to drag ratio of just the body. However, this will change based on cruise sizing of the missile when lifting surfaces are added. Although, 11 degrees cruise angle of attack gives the best lift to drag ratio for the WRAITH. At Mach 0.7 and 1.3 degrees, the lift to drag ratio is determined to be 0.4. The lift to drag ratio per angle of attack is shown in Figure 19.

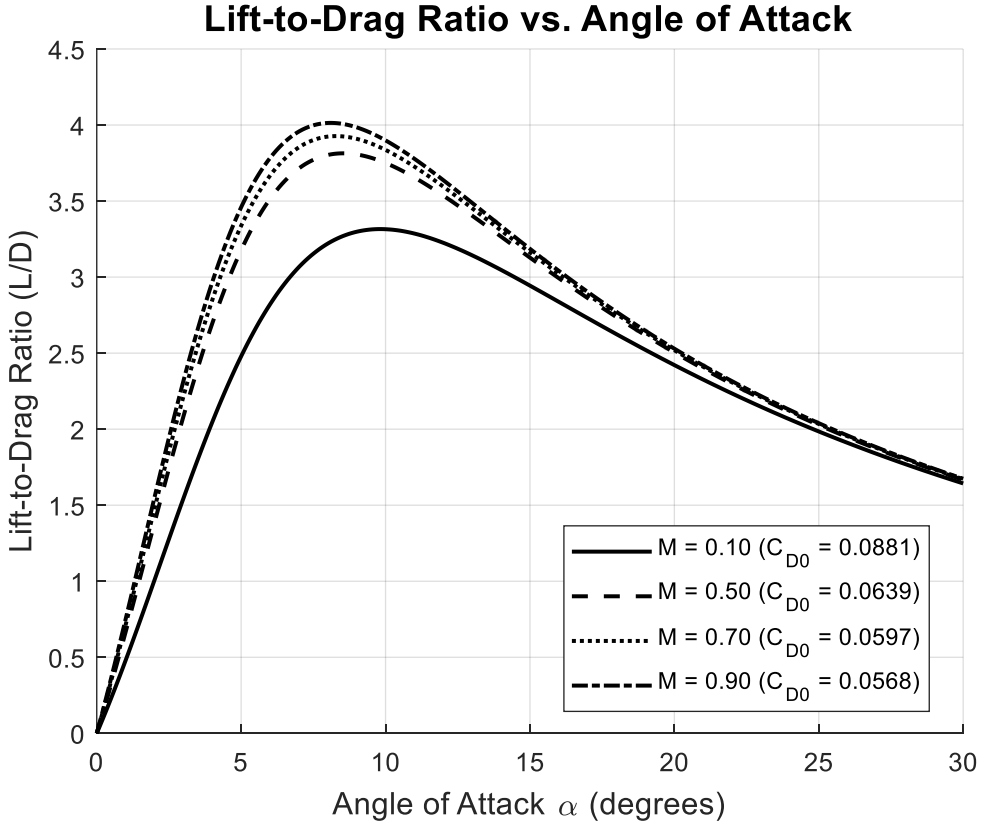

Figure 19 Body L/D over different Angles of Attack and Mach number

From Table 2, the body L/D ratio grows with an increase of α within the range of 0 - 10 deg. After this point, the drag increases more rapidly than lift, which results in a decline in the L/D ratio. This effect is explained mathematically by the following equation showing the increase in as the C_{D_0} increases.

$$\frac{L}{D} = \frac{C_L}{C_D} = \frac{(C_N \cos\alpha - C_{D_0} \sin\alpha)}{(C_N \sin\alpha + C_{D_0} \cos\alpha)}$$

The missile body alone achieves a lift to drag ratio of 3.93 at angle of attack near 10 degrees and a cruise Mach number of 0.71. These results provide a baseline of the body lift efficiency and highlight the importance of including a lifting surface to enhance the missile aerodynamic performance.

IX. Cruise Flight

Cruise conditions:
Altitude: 2,000 ft
Mach Number: 0.7
Cruise AoA: $\alpha = 0.5°$

The cruise performance test for the missile was conducted to determine if the body and wing configuration can sustain a steady level flight at a lower altitude. In this analysis we chose a 2,000 feet altitude with a Mach number of 0.7 representing a subsonic long-range cruise. For this missile the design constraint is that at an $\alpha < 10$ The lift generated by the missile must equal the weight of the missile. Normal force coefficient and drag coefficient were calculated in previous sections and used here.

To calculate the lift coefficient both normal and drag coefficient were used in the following formula.
$C_L(\alpha) = C_N(\alpha)cos\alpha - C_{D0,tot}sin\alpha$

The dynamic pressure at 10,000 ft and Mach 0.7 is calculated in standard atmosphere and used to calculate the lift in the following equation.

$L(\alpha) = C_L(\alpha)qS_{ref}$

Table 3 cruise condition and results

Parameter	Values
Altitude	2,000 ft
Mach number	0.71
Weight (W)	2,250 lbf
Tail area (S_{tail})	3.36 ft^2
Wing area (S_{Wing})	7.87 ft^2
Tail area (S_{Tail})	3.64 ft^2
Cruise satisfied at α	0.5°

Figure 20 shows the lift per angle of attack and required cruise angle of attack

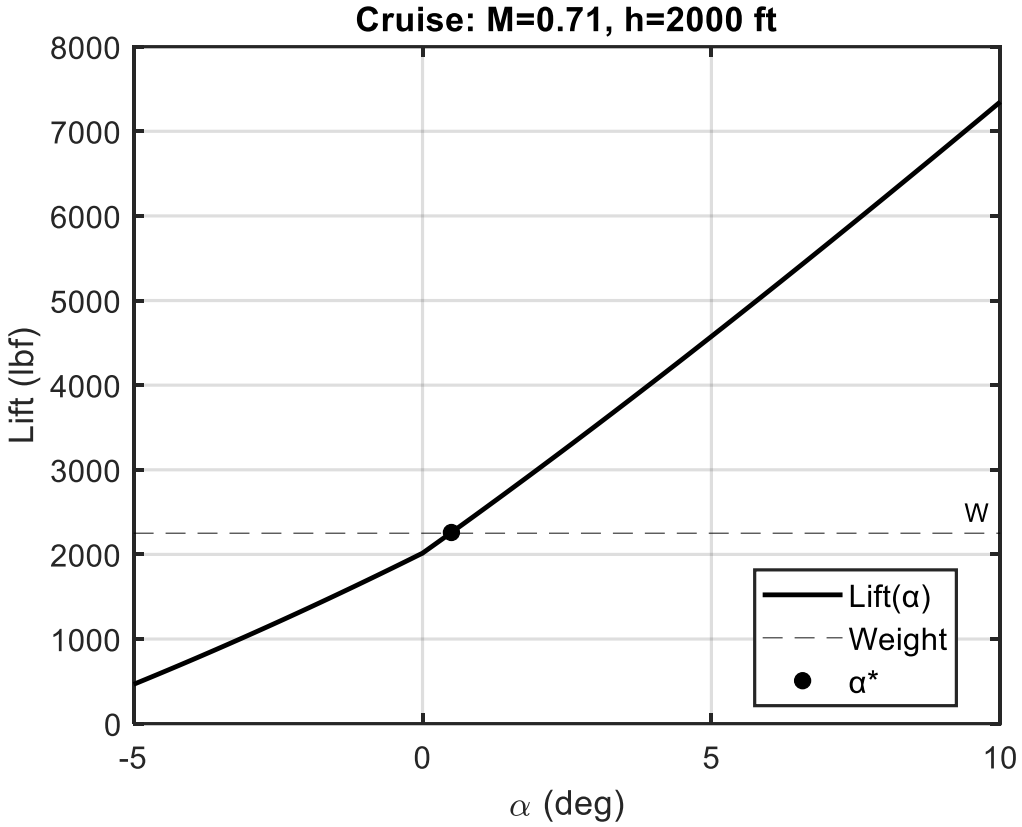

Figure 20 Cruise Lift per Angle of Attack

From Table 3 the missile body and wing surface satisfies the required cruise conditions at an angle of attack of $\alpha = 0.5°$ as that the missile will generate lift equal to the weight at that angle. Within $\alpha < 10°$ the maximum lift generated is almost 8,000 lbf indicating that the missile design has sufficiently generated lift.

The angle of attack at which the cruise is achieved shows that the chosen wing geometry is adequate for a Mach 0.71 cruise in a lower atmosphere. The fuselage does generate lift, but the addition of lifting surface is required to reduce the α into a practical operating range.

X. Tail Sizing

The tail was redesigned to accommodate a vee-tail configuration with two surfaces angled with a 60-degree dihedral. The tail was sized so that with a set center of gravity of 6.46 feet from the nose, the static margin of the missile was equal to zero, shown in the equation below:

$$S.M. = \frac{X_{AC} - X_{CG}}{\mathrm{d}}$$

The vertical and horizontal contribution of a dihedral tail were determined using the equation below.

$$(S_{VT})_{eq} = S_T \, sin^2(\phi)$$

$$(S_{HT})_{eq} = S_T \cos^2(\phi)$$

With S_T being tail area and ϕ defined as the dihedral angle. Determining this relationship, the equivalent horizontal tail area was sized to meet the neutral static margin requirement. The equation to define the required horizontal tail area is defined below.

$$S_{HT} = \left\{ \left(C_{N_\alpha}\right)_B \frac{x_{CG} - (x_{AC})_B}{d} + \left(C'_{N_\alpha}\right)_W \left[\frac{x_{CG} - (x_{AC})_W}{d}\right] \left(\frac{S_W}{S_{Ref}}\right) \right\} \frac{d}{(x_{AC})_T - x_{CG}} \frac{S_{Ref}}{\left(C'_{N_\alpha}\right)_T}$$

Using the aerodynamic centers determined earlier, the equivalent horizontal tail area was calculated and graphed over the flight envelope, then, using the relationship established previously, the tail area was determined, shown in Figure 21.

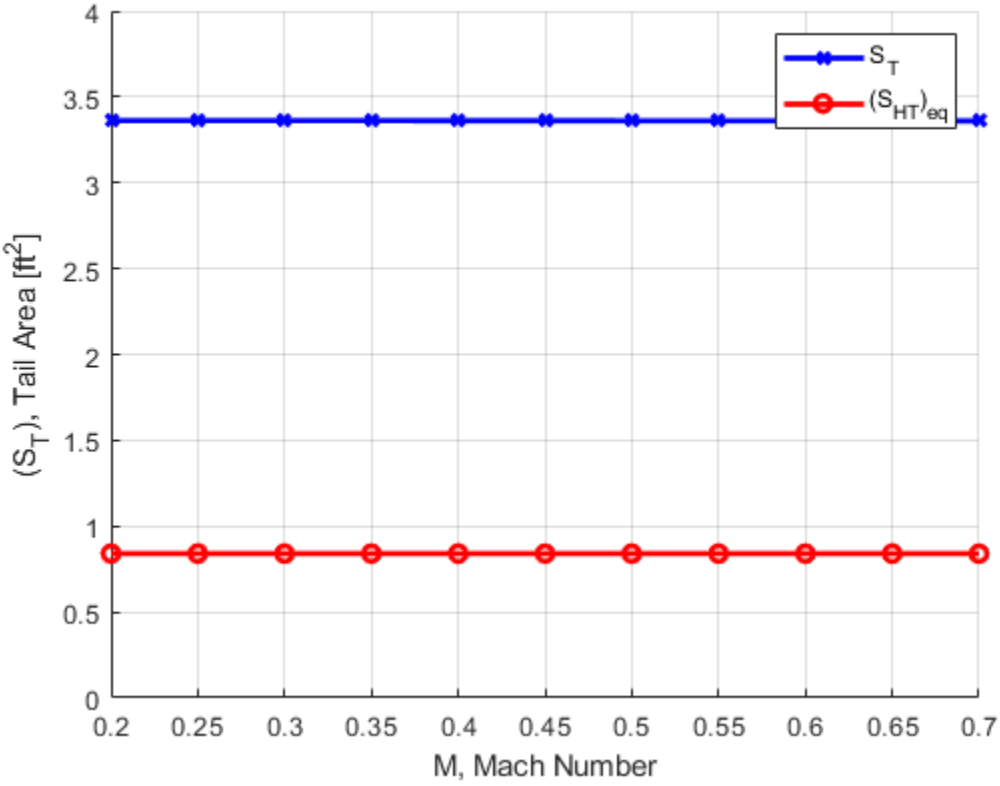

Figure 21 Required Tail Area

For a cruise speed of Mach 0.7, the required tail area and equivalent horizontal tail area was determined using the method detailed above. The resulting tail geometry is summarized in Table 4.

Table 4 Redesigned Tail Geometry

Table 4 Redesigned Tail Geometry

$b_T\ [ft]$	$(c_r)_T\ [ft]$	$(c_t)_T\ [ft]$	$\phi[deg]$	$S_T\ [ft^2]$	$(S_{VT})_{eq}\ [ft^2]$	$(S_{HT})_{eq}\ [ft^2]$
2.4	1.5	1.3	60	3.36	2.52	0.84

The resulting geometry required to achieve a neutral static margin is shown in Figure 22. The redesigned vee-tail consists of a wide-spaced pair of surfaces canted at 60°, providing both pitch and yaw control through coupled control surfaces. This configuration shifts the aerodynamic center rearward and increases the moment arm relative to the missile's center of gravity, allowing for neutral stability without a significant increase in tail area. The 60° dihedral was selected as an optimal balance between control effectiveness and minimizing the tail footprint.

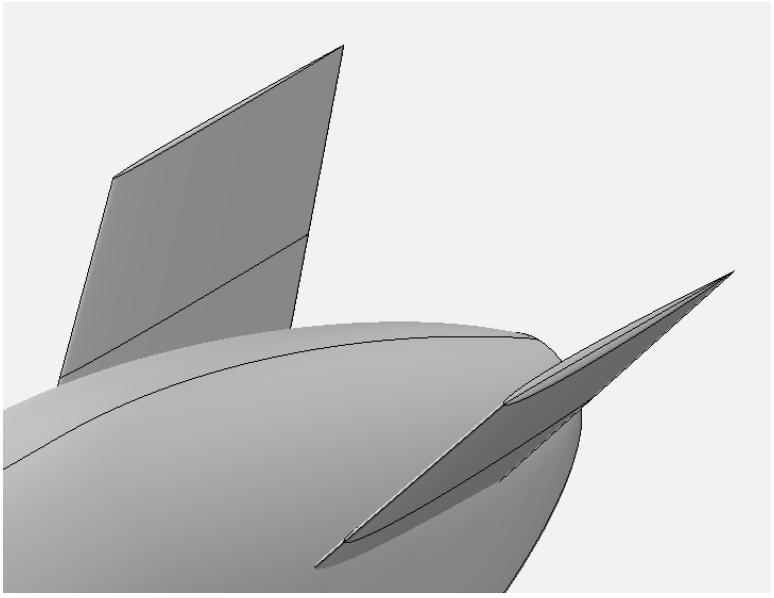

Figure 22 WRAITH Tail Geometry

To maintain the dimensional and storage requirements, the redesigned vee-tail incorporates a folding mechanism that allows it to collapse inward, reducing the overall footprint of the missile. This feature significantly improves storage and handling efficiency, particularly in confined environments such as internal weapon bays or transport containers. The folding motion is achieved through a hinged assembly located at the tail root, enabling the fins to rotate inward without interfering with the main body structure or adjacent components. The resulting stowed tail configuration is shown in Figure .

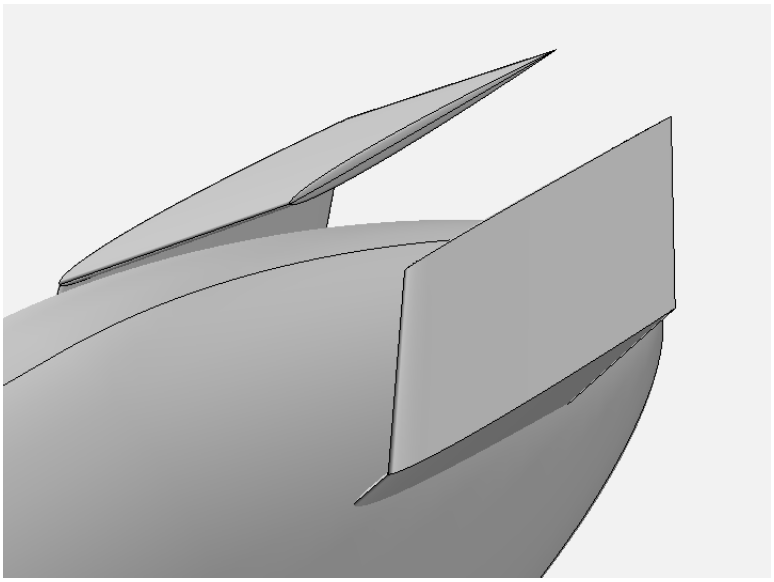

Figure 23 Stowed Tail Configuration

v

XI. Aerodynamic Redesign Summary

The updated aerodynamic configuration is shown in Figure 24. This design incorporates two major changes: an increased wingspan and a redesigned tail. The larger wing planform is intended to generate higher lift and improve cruise efficiency, which directly supports extended range and improved terminal maneuverability. In addition, the tail surfaces were reworked to provide more effective control authority while maintaining stability across the operating envelope.

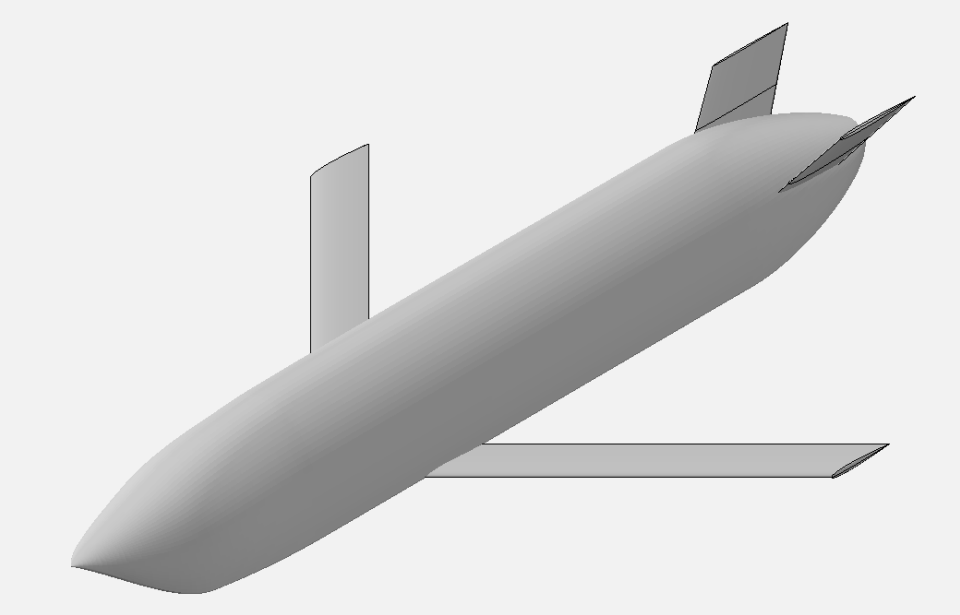

Figure 24 WRAITH Aerodynamic Redesign

Figure 25 shows the missile in its stowed configuration. In this state, the wings are retracted, and the tail surfaces are folded against the body. This reduces the overall span and projected area of the vehicle, allowing it to fit within existing storage, handling, and launch interface constraints.

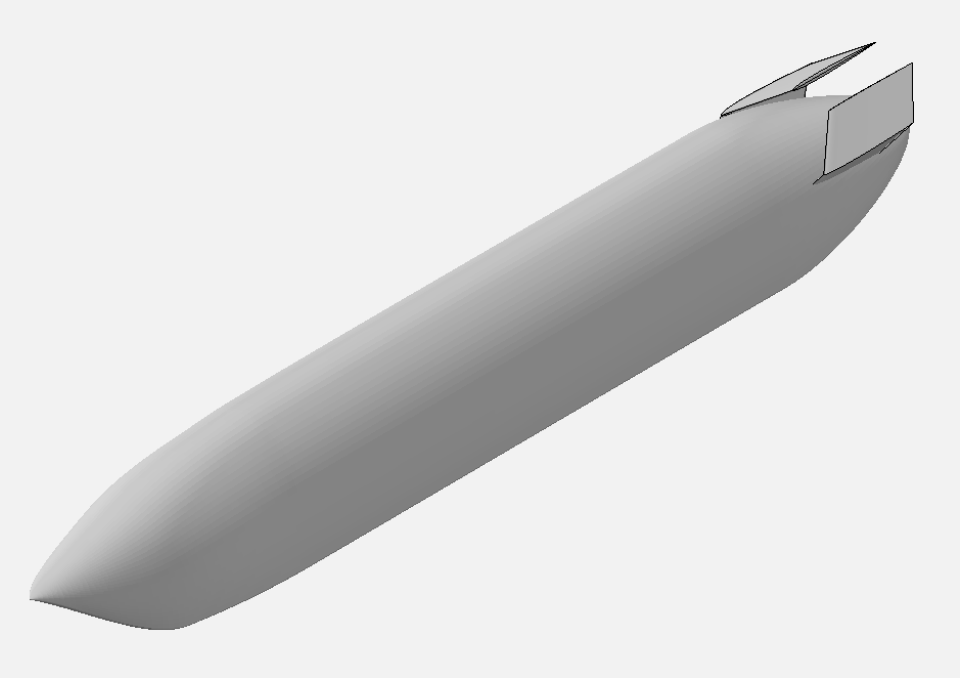

Figure 25 WRAITH Stowed Configuration

XII. References

[1] Svitlyk, Y. "AGM-158 JASSM: Joint Air-to-Surface Standoff Missile." Root Nation, November 25, 2024. https://root-nation.com/en/articles-en/weapons-en/en-agm-158-WRAITH-air-launched-cruise-missile/

[2] Siemens Digital Industries Software, *NX* [computer software], Version 2306, Siemens Digital Industries Software, Plano, TX, 2023. URL: https://www.plm.automation.siemens.com/global/en/products/nx/

[3] USAF launches JASSM New Variant Missile. Default. (n.d.). https://www.janes.com/osint-insights/defence-news/weapons/usaf-launches-WRAITH-new-variant-missile

[4] UPDATED JASSM® completes important Lockheed martin flight tests. Media - Lockheed Martin. (n.d.). https://news.lockheedmartin.com/2017-03-08-Updated-JASSM-R-Completes-Important-Lockheed-Martin-Flight-Tests

[5] U.S. Standard Atmosphere, 1976, NOAA-S/T-76-1562, NASA-TM-X-74335, National Oceanic and Atmospheric Administration, Washington, D.C., Oct. 1976. Available: https://www.robertribando.com/xls/fluid-mechanics/1976-u-s-standard-atmosphere/

[6] Fleeman, E. L., & Schetz, J. A. (2012). *Missile Design and System Engineering*. American Institute of Aeronautics and Astronautics.

[7] OpenVSP, *Open Vehicle Sketch Pad (OpenVSP), Version 3.33.0*, NASA Open Source Software, 2025. Available: https://openvsp.org

[8] Drela, M. Flight Vehicle Aerodynamics. Cambridge, MA: MIT Press, 2014.

[9] The MathWorks Inc., *MATLAB, Version 9.15.0 (R2024b)*, Natick, MA, 2024. Available: https://www.mathworks.com

XIII. Appendix A Paragraph Contributions

- Tri Phan
    - Lift-over-Drag, Cruise Flight
- Nathaniel Hollman
    - Body Drag, Normal force, and aerodynamic center. Total Lift and Drag.
- Tiger Sievers
    - Mean Aerodynamic Center, Tail Lift and Drag, Tail Sizing
- Mohammed Almazrouei
    - Wing Drag, Normal Force, and aerodynamic center.

XIV.Appendix B